Zhang, C., Heiselberg, P.K., Chen, Q., and Pomianowski, M. 2017. "Numerical analysis of diffuse ceiling ventilation and its integration with a radiant ceiling system," *Building Simulation*, 10(2): 203-218.

Numerical analysis of diffuse ceiling ventilation and its integration with a radiant ceiling system

Chen Zhang[a,*], Per Kvols Heiselberg[a], Qingyan Chen[b], Michal Pomianowski[a]

[a] Department of Civil Engineering, Aalborg University, Sofiendalsvej 11, 9200 Aalborg, Denmark

[b] School of Mechanical Engineering, Purdue University, West Lafayette, IN 47907, USA

*Corresponding author's Tel: +45 9940 7232; E-mail: cz@civil.aau.dk

Abstract

A novel system combining diffuse ceiling ventilation and radiant ceiling was proposed recently, with the aim of providing energy efficient and comfort environment to office buildings. Designing of such a system is challenging because of complex interactions between the two subsystems and a large number of design parameters encountered in practice. This study aimed to develop a numerical model that can reliably predict the airflow and thermal performance of the integrated system during the design stage. The model was validated by experiments under different operating conditions. The validated model was further applied to evaluate the effects of different design parameters, including the U-value of the diffuse ceiling panel, plenum height, plenum depth, and inlet configuration. In the integrated system, diffuse ceiling separated the radiant ceiling from the rest of the room and consequently changed the energy efficiency of the radiant system. The simulated results demonstrated that using ceiling panel with a higher U-value can minimize this impact and make the system to cool down space efficiently. Low plenum height was beneficial to the energy efficiency, but aggravated the non-uniformity air distribution and further led to the draught problem in the occupied zone. This system was recommended to apply in the small offices instead of large, open spaces.

Keywords

Diffuse ceiling ventilation, Radiant ceiling, CFD, Parametric study, Thermal comfort, Energy efficiency

1. Introduction

Recently, a growing interest has been paid on a new ventilation system - diffuse ceiling ventilation. This ventilation concept uses an open space between ceiling slab and suspended ceiling as a plenum to distribute air. The conditioned air is delivered to the room through the perforations on the suspended ceiling panels and/or slots between ceiling panels. Compared with traditional ventilation systems, diffuse ceiling ventilation has a potential to provide a more comfort environment with less energy cost. Because of the large ceiling area as air diffuser, the system has low- momentum supply flow and does not generate draught even by supplying cold outdoor air directly (Jacobs et al. 2009; Fan et al. 2013; Nielsen et al. 2009). This ventilation concept is appropriate to the spaces with high thermal load and large ventilation demand, like offices and classrooms, where draught is usually a major concern by using conventional mixing or displacement ventilation (Hviid and Svendsen 2013). On the other hand, the suspended ceiling as air diffuser requires low-pressure drop due to its large surface area. The use of plenum eliminates the need for ductwork and the large size of the plenum creates a little restriction to the air flow (Bauman 2013). Consequently, this ventilation

system requires less energy for the fan than the fully ducted systems (Hviid and Svendsen 2013; Jacobs et al. 2008; Jakubowska 2007). However, ventilation is a passive cooling approach, determined by the outdoor climate. An additional heating and/or cooling system is necessary when natural resources are inadequate. Radiant ceiling is a promising solution to work together with ventilation systems. Because it deals with heat load by both radiation and convection, which could provide a more comfort environment than the all-air system and able to make use of low-grade energy (Su et al. 2015; Arcuri et al. 2015; Niu and Kooi 1994).

A schematic diagram of the system combined diffuse ceiling ventilation with radiant ceiling is shown in Figure 1. In the integrated system, the suspended ceiling covers the radiant ceiling and consequently changes the heat transfer mechanism between the radiant surface and the rest of the room. Initial investigations have been done by full-scale experiments under steady-state conditions (Zhang et al. 2015a; Yu et al. 2015). The results indicated that the diffuse ceiling ventilation increased the heating capacity of radiant ceiling but decreased its cooling capacity. The thermal process in the plenum was more complicated than that in the ducted systems. The direct contact between the supply air and the radiant ceiling enabled heat transfer to or from the air depending on the air-to-surface temperature difference and airflow rate, which resulted in a temperature variation on the plenum air. From the standpoint of thermal comfort, due to the preheating/precooling effect of the plenum, air was supplied into the room with moderate temperature, which further reduced the risk of draught. The previous investigations showed that the diffuse ceiling ventilation and the radiant ceiling interact and complement with each other. Therefore, the system needs properly design and control, to fulfill both energy saving and thermal comfort purposes.

Figure 1

The most common integrated system in practice is displacement ventilation with cooled ceiling. This combined system gives a rather superior performance on the air quality and thermal comfort to the VAV system (Niu and Kooi 1994; Novoselac and Srebric 2002). However, the harmony of the combination is the key issue, since cooled ceiling creates a downward motion of air and suppresses the displacement flow. Therefore, the amount of heat load removed by cooled ceiling needs be properly adjusted in order to maintain a low vertical temperature difference and a high air quality in the breathing zone (Rees and Haves 2013; Brohus 1998). At the same time, the entire cooling load needs to be lower than 100 W/m^2, and the room height is required to be higher than 2.5 m (Riffat et al. 2004). The possibility of radiant floor and displacement ventilation was discussed by several studies (Causone et al. 2010; Krajčík et al. 2013). They mentioned that floor cooling did not lead to an increase in draught risk, but vertical temperature gradient must be controlled carefully in the cooling case. Although the integrations of ventilation and radiant systems have been widely studied, the knowledge regarding the combination of diffuse ceiling ventilation and radiant ceiling is very limited.

As mentioned above, the design of such an integrated system is challenging due to the interactions between its two subsystems. In this study, the primary objective was to optimize the energy performance of the radiant ceiling and provided a more uniform air distribution through the diffuse ceiling. The design process would need to define a large number of parameters, such as diffuse ceiling configuration, plenum geometry, shape and location of the plenum inlet, obstruction within the plenum, etc., which would have impacts on these interactions. To explore the effect of different design parameters, one can use experimental and/or numerical approaches. Experimental study is regarded to be more reliable but also more expensive and time-consuming than numerical investigation. Therefore, it is desirable to develop a validated numerical model that could provide a reliable prediction of the integrated system during the design stage.

Numerical evaluation on the two subsystems has been reported in many articles. For diffuse ceiling ventilation, Fan et al. (2013) simplified the diffuse ceiling supply into four slot openings. They observed disparities in the air velocity distribution, especially near the ceiling and the floor. The disparities were because the simplification of the air pathway resulted in an overestimation or underestimation of the air movement in the conditioned space. Chodor et al. (2013) assumed the outdoor air directly supplied into the room without going through the plenum, and they also assumed a uniform air distribution through the suspended ceiling. They oversimplified the inlet boundary conditions and neglected the thermal process within the plenum, which led to a discrepancy in the airflow prediction inside of the room. Zhang et al. (2016) proposed a porous media model, which could efficiently predict the airflow characteristics through the diffuse ceiling panels. However, this study focused on the airflow pattern in the conditioned space, and no detail discussion regarding the plenum was available. For the radiant ceiling system, Tye-Gingras et al. (2012) coupled a semi-analytic radiant model with a 2D CFD model to analyze the comfort and energy consumption of the radiant ceiling. However, this study neglected the impact of ventilation on the airflow pattern, and only considered the buoyancy force from heat sources. Myhren et al. (2008) used a validated CFD model to compare different radiant heating systems, where a surface-to-surface method was implemented to deal with the radiation heat exchange. The previous studies mainly focus on the individual system, but the study regarding the integrated system was limited. In addition, the air distribution and thermal process within the plenum should also be addressed in this study, where the heat exchange between radiant ceiling and supply air mainly takes place.

This study aimed to develop a validated numerical model for the system with diffuse ceiling ventilation and radiant ceiling. This model should be able to predict the airflow pattern and thermal performance both in the plenum and in the occupied zone. This investigation further used the validated model to conduct a series of parametric studies, including the U-value of the diffuse ceiling panel, plenum height, plenum depth, and plenum inlet configuration, for optimal design of the integrated system. It needs to notice that both the experiments and numerical simulations presented in this study were conducted under steady-state condition, where the effect of thermal masses (ceiling slab and suspended ceiling) was not the focus of this study.

2. Experimental setup

To develop a validated numerical model, we needed reliable and high-quality experimental data. This section describes the experimental facility and the measurement technique.

2.1 Test facility

The full-scale experimental facility was an environmental chamber located inside a laboratory. As illustrated in Figure 2, the environmental chamber consisted of two parts: a climate chamber simulating the outdoor environment and a test chamber simulating an office with a ceiling plenum. The office had an inner dimension of 4.8 m × 3.3 m × 2.72 m. The office layout included two workstations with two PC, two lamps as well as two thermal manikins (Figure 3), which corresponded to a heat load of 450.5 W or 28.4 W/m2 floor area.

Figure 2

Figure 3

There were two glazing areas in the façade between the climate chamber and the test chamber. The lower glazing area, with three panels and overall dimensions of 2.4 m × 1.4 m, was closed during the experiments.

The upper glazing area, with three panels and overall dimensions of 2.4 m × 0.35 m, was opened to function as plenum inlets. The inlet opening could be controlled by adjusting their opening angle, and it kept a geometrical opening area of 0.0207 m^2 (0.01 m × 0.69 m × 3 panels). The exhaust duct was in the lower corner of the façade and had 160 mm diameter. The exhaust air was drawn into the climate chamber using a fan, and then treated by an AHU unit when it passed through the climate chamber, finally re-supplied to the plenum. The façade had an effective U-value of 0.61 $W/m^2.K$ and the other enclosures were well insulated to minimize the heat transfer from the lab.

2.2 Diffuse ceiling and radiant ceiling

The diffuse ceiling panels were the type of wood-cement panels typically used for acoustic purposes, but they were permeable to air. The ceiling panels were positioned 0.35 m below the ceiling slabs by a suspension system, which separated the test chamber into a ceiling plenum and a conditioned space as shown in Figure 4. The diffuse ceiling panels had a thickness of 35mm and a density of $359kg/m^3$. The thermal conductivity of the ceiling panels, measured with a λ-Meter EP500 by a guarded hot plate method, was 0.085 W/m K. The porosity was estimated to be 65% by means of a volumetric measurement. The high porosity ensured a low-pressure drop across the ceiling panel. According to previous measurements (Zhang et al. 2015b), the pressure drop through the diffuse ceiling was less than 2 Pa when the airflow rate was less than or equal to 0.03 $m^3/s{\cdot}m^2$. Since there were small cracks between the ceiling panels, the pressure drop across the whole diffuse ceiling was even lower.

Figure 4

The radiant ceiling was composed of four concrete slabs with embedded water-carrying pipes, each with dimensions of 3.560 m × 1.197 m × 0.200 m. The water pipes with a diameter of 20 mm were embedded 4 mm above the lower surface of the concrete slab. The water circuit connected to both heating and cooling units, where a three-way valve used to control the water temperature. The water flow was controlled and recorded by a Brunata HGQ flow meter.

2.3 Case setup

Measurements were conducted for three cases with different boundary conditions, as shown Table 1. In winter, the radiant ceiling was operated as a heated ceiling with a surface temperature of 27.34 ºC. In moderate seasons, the radiant ceiling was not activated, and ventilation was used to remove the load for the entire space. While in summer, radiant ceiling took charge of the whole heat load and ran with a surface temperature of 10.79 ºC. The radiant surface temperature was below the dew point temperature in summer, and there was a risk of condensation in practice. However, the experimental study aimed to identify the possibility and limitation of the integrated system, even the case with condensation risk was still tested.

Table 1

The experiments focused on the airflow and thermal performance in both the plenum and the occupied space. The vertical temperature gradient and velocity gradient in the office were measured with the use of three moveable poles, in each pole located seven thermocouples and five anemometers, as shown in Figure 5 (a). During the experiment, each pole was moved to four different positions within the office, so that the measurements were conducted at a total of 12 locations in the occupied zone. Figure 5 (b) shows the measuring points in the plenum. A total of nine thermocouples were evenly distributed at the mid-height of the plenum to measure the temperature variation of plenum air. The surface temperatures of the walls, floor, radiant ceiling, and diffuse ceiling panels were also measured. The experiment used 115 K-type thermocouples for monitoring the air and surface temperatures, with an uncertainty of ± 0.15 K. The

thermocouples measured the temperatures every 10 s, and the data was recorded by a Helios Fluke data logger. The velocities were measured by the hot-sphere anemometers with an uncertainty of ± 0.01 m/s +5% of the readings. The air velocities were recorded by a 54N10 Dantec multichannel flow analyzer.

Finally, the pressure drop through the diffuse ceiling was measured with FCO510 micro-manometers (uncertainty ± 0.25 %) by placing the pressure sensors at various locations in the plenum and in the center of the office, as shown in Figures 5. Detailed information about the measurements was described in Zhang et al. (2015a) and Yu et al. (2015).

Figure 5

3. Numerical models

The numerical study used a CFD model to solve the airflow and temperature distributions in the plenum and the occupied space. The commercial CFD programme Fluent (ANSYS Inc. 2015) was used in this study. The CFD simulations require a suitable model to specify the airflow through the diffuse ceiling panels. As the radiant ceiling has a large temperature difference from the rest of the surfaces in the room, a suitable radiation model is essential to analyse the radiative heat transfer in space. This effort would provide the necessary boundary conditions for the porous media model. The CFD model also requires a suitable turbulence model for solving the airflow and temperature distribution in the occupied space. This section discusses the numerical models used for the investigation.

3.1 A porous media model for the diffuse ceiling panels

The diffuse ceiling panels used in this study had a porous property because of the structure of the wood-cement material. It was impossible to model the air diffusion through the panels directly. A porous media model was implemented to simulate the air diffusion in this study. As flow through the porous media zone, it experiences both the viscous resistance and inertial resistance. The porous media model was developed by adding a momentum source term in the governing equation, based on Darcy-Forchheimer Law (ANSYS 2009). When the flow goes through the porous panels with very low velocity, the viscous term is dominant. However, for high-velocity flow, the inertial effect becomes significant. The momentum source term can be expressed by:

$$S_M = -\left(\frac{\mu}{\alpha}v + C_2\frac{1}{2}\rho|v|v\right) \qquad (1)$$

The viscous resistance coefficient $1/\alpha$ and inertial resistance coefficient C_2 were determined by the properties of the wood-cement board, such as porosity and equivalent perforation diameter. These two coefficients were derived from experimental data in the form of pressure drop as a function of velocity through the porous media, where $1/\alpha = 1.14 \times 10^8$ m^{-2} and $C_2 = 33055$ m^{-1}. Detailed information about pressure drop measurement and results can be found in Zhang et al. (2015b).

The energy equation for the porous panels was modified on the conduction flux only, where an effective thermal conductivity k_{eff} was introduced to consider the effect of both the fluid and solid conductivities.

$$\nabla \cdot \left(\bar{v}(\rho_f E_f + P)\right) = \nabla \cdot \left[k_{eff}\nabla T + (\bar{\tau} \cdot \bar{v})\right] + S_E \qquad (2)$$

$$k_{eff} = \gamma k_f + (1-\gamma)k_s \qquad (3)$$

3.2 Radiation model

Radiative heat transfers occur between the radiant ceiling, diffuse ceiling panel and the rest of the room surfaces. Unfortunately, our CFD program with the porous media model treated the diffuse ceiling panel as flow cells and thus could not calculate the radiative heat exchange directly. In order to determine the

radiative heat exchanges, a separate model was built by specifying the diffuse ceiling panels with the corresponding solid materials. A surface to surface method was implemented to calculate the radiative heat transfer between surfaces by use of the Stefan-Boltzmann law and view factors. The radiative heat flux leaving a given surface is expressed (ANSYS 2009):

$$q_{rad,k} = \varepsilon_k \sigma T_k^4 + \rho_k \sum_{j=1}^{N} F_{kj} q_{rad,j} \qquad (4)$$

In the radiation model, the wall boundaries were specified by the U-value together with the outdoor temperature or called free stream temperature. The radiant ceiling was specified by a uniform surface temperature, and the temperature decay along the pipe was assumed to be negligible (less than 3 ^{o}C in the measurements). The internal heat sources were treaded as surface heat fluxes on the manikins, computers, and task lamps.

The calculated results obtained from the radiation model included the surface temperatures of the walls and radiative heat flux of the diffuse ceiling panels.

3.3 Boundary conditions

The wall temperatures obtained from the radiation model were then used as boundary conditions in the porous media model for the detail calculation on the air velocity and air temperature distribution. Instead of directly specifying the diffuse ceiling's surface temperature, the radiative heat flux to the diffuse ceiling panels was applied as an energy source S_E.

The heat sources released heat through both convection and radiation. The effect of radiative heat flow has been already considered in the radiation model. A feasible approach was to estimate the radiative heat flow and to specify the convective heat flow boundary condition for the heat sources (Srebric and Chen 2002). ASHRAE Handbook (2009) provides default convective fraction for different heat sources. The convective fraction of occupants with moderately active office work was approximate 50%, while the values of computers and desk lamps were 90% and 50%, respectively.

3.4 Turbulence model

The airflow through diffuse ceiling panels could be laminar because of the very low velocity. However, the room airflow was turbulent because of strong thermal plumes from various heat sources and convective heat transfer through the room enclosure. The Re-normalized group (RNG) k-ε model was recommended by Chen (1995) to model the turbulent flow in the indoor environment. Yang et al. (2008) also proved the accuracy of the k-ε model for the porous media zone.

3.5 Geometrical model

The geometrical model used in CFD, as shown in Figure 6, was a simplified version of the environmental chamber facility. This model included the plenum, the diffuse ceiling, and the occupied office. The three lower glazing panels were consolidated as a window and the three upper glazing panels into an inlet. A ventilation duct located in the lower left corner of the façade was treated as an exhaust. In order to generate high-quality meshes for the indoor space, the inlet and exhaust were built as rectangular openings with the effective areas as in the experiment. The air supply through the inlet was assumed to have a uniform profile. The exhaust was treated as outflow boundary with zero diffusion flux for all flow variables.

Figure 6

3.6 Numerical algorithm for CFD

As shown in Figure 6, structured meshes were built in the entire space. The finest meshes were generated in the areas with large gradient, for example, the diffuse ceiling, inlet, outlet, walls, and heat sources. Chen et al. (2002) recommended systematically refining the grid size to verify the numerical model. A common approach is to double the mesh number and then to compare the two mesh solutions. Three mesh solutions were constructed in the grid independent study, and the results for exhaust air temperature and average air velocity at position A2 are presented in Table 2. The comparison indicates that the calculation with Mesh 2 produced accurate results for air velocity at A2, and the deviation in exhaust air temperature was less than 0.11% with Mesh 3. The increase in cell number from 760,235 to 1,027,309 did not result in a significant improvement in the simulated results, but cost more computing time and needed larger computational resources. Consequently, Mesh 2, with 760,235 cells, was used for further investigation in this study.

The solution method was the SIMPLE algorithm. The convergence criterions were set that the absolute residuals should be less than 10-3 except that for energy less than 10-6. Table 2 shows the unbalance rate for mass and heat flux, where the mass reached a complete balance state and the heat flux unbalance in the range of 0.09%–0.2%.

Table 2

4. Model Validation

In this section, we will present the computed airflow pattern for the test chamber with the integrated system and compare the calculated temperature and velocity distributions with the corresponding experimental data. The objective is to validate the numerical model for predicting the performance of the integrated system.

4.1 Temperature distribution

Figure 7 illustrated the computed temperature distributions in the room with the integrated system. A clear temperature difference between the plenum and the conditioned space was observed in all cases. The temperature difference was due to the positive pressure in the plenum prevents the mix of the plenum air and the room air, at the same time, the diffuse ceiling panels served as a layer of insulation maintains the temperature difference between the two zones. On the other hand, although the air was supplied through the diffuse ceiling with uneven temperature, the impact on the temperature distribution in the room was not significant. The air was predicted to be uniformly distributed in the occupied zone with the help of the convective flow from heat sources. A slight displacement tendency was observed, where the warmest air layer occurred just below the diffuse ceiling. The displacement effect of diffuse ceiling ventilation was mentioned by Petersen et al. (2014), they found out that a tendency of displacement effect occurs at low heat loads and development towards fully mixing with increasing of heat loads.

Figure 7

Figure 8 showed the comparison between the calculated temperatures and the measured ones at position A2. The numerical model provided a satisfactory prediction on the air temperature in the occupied zone, with deviations less than 0.36 ^{o}C. The largest deviation occurred below the diffuse ceiling. The CFD model seems to overestimate the effect of the thermal plume generated by the heat sources, which led to a 2 ^{o}C higher air temperature in this region. It is well known that the wall function used in the RNG k-ε model cannot correctly predict the convective heat transfer at solid surfaces. Therefore, to keep the calculated results sufficiently close to the measured ones for exhaust and average air temperatures, a high convective fraction

was applied to specify the thermal boundary of the heat sources. In addition, the measurements were not free from errors, which could also have contributed to the discrepancy.

Figure 8

In the integrated system, complex thermal processes take place within the plenum. Therefore, the numerical model should be able to provide a reliable prediction in the plenum. Figure 9 presented the horizontal temperature distribution at the mid- height of the plenum for the three cases. It was clear that the CFD model can predict the relation between air temperature variation and the distance from the plenum inlet. Although the deviations between the simulated temperatures and measured ones can reach 2 ^{o}C in some points, if consider the large temperature range of the supply air from -7 ^{o}C to 24 ^{o}C, the deviations can be regarded as acceptable. In winter, the cold outdoor air entered the plenum from the left. As it passed through the plenum, it was gradually warmed up by the heat transferred from the radiant surface on the top and from the diffuse ceiling panel on the bottom (heat conducted from the room side). In summer, by contrast, the air in the plenum was gradually cooled down by cooled ceiling. In the moderate season, although the radiant ceiling was not activated, the air was still warmed up by heat transfer from the upper zone and the room side.

Figure 9

4.2 Air flow pattern and velocity distribution

Figure 10 illustrates the computed velocity distribution in the three cases. The rising buoyancy flow from the heat source and the downward flow along the wall generated an air recirculation in the room and caused reverse flow entering the occupied zone along the floor. In different cases, the vortex moved from one side of the room to the other depending on the operating conditions. In winter, the outdoor air was supplied to the plenum at a low temperature, and because of gravity, a large amount of air dropped to the surface of the diffuse ceiling and penetrated into the room at a location close to the plenum inlet. In contrast, warm supplied air could travel further in the plenum and was gradually cooled down by the thermal mass. Therefore, a relatively large amount of air was delivered to the room at the far end. This phenomenon explains the fact that the air distribution through the diffuse ceiling was not perfectly uniform, which depended on the supplied air condition and the thermal process within the plenum.

Figure 10

Figure 11 showed the calculated and measured velocities at position A2. Overall, good agreements have been reached on the velocity results. However, a relative larger discrepancy existed below the diffuse ceiling. As mentioned above, the discrepancy was due to the overestimation of the convective flow from the heat sources. Both calculated and measured results showed low air velocities in the occupied zone by using this system. A relative higher velocity occurred at the floor level in the winter case. However, it was still lower than the limit of 0.18 m/s (CEN 1998), no draught risk would be expected.

Figure 11

5. Parameter analysis

Most of the previous studies have pointed out the need to expose the radiant ceiling to the rest of the room to optimize the energy efficiency. However, in the integrated system, the radiant ceiling is encapsulated by the diffuse ceiling panels. Therefore, the properties of diffuse ceiling panels have a remarkable impact on the thermal performance of radiant ceiling. Two different diffuse ceiling panels were analyzed: one was wood-cement panel as used in the experiment, and the other was aluminum (Al) panel. The Al panel was

chosen as an example because it is the most commonly used type of suspended ceiling in practice, and it has significantly higher U-value than does wood-cement panel. The Al panel was expected to perform differently from the wood-cement panel.

On the other hand, from an architectural standpoint, it is preferable to reduce plenum height in order to maintain sufficient headroom. It is important to identify the minimum plenum height at which an acceptable air distribution within the plenum could be achieved. Plenum depth is also an important parameter because airflow may not reach the end of the plenum if the depth exceeds a certain value. Finally, the plenum inlet configuration and location determine the momentum of supply air and the airflow pattern in the plenum.

This study aimed to identify the impact of different design parameters on the thermal performance and airflow pattern in the room with the integrated system. The study used the validated CFD model for investigating the sensitivity of the design parameters, including the U-value of the diffuse ceiling panel, plenum height, plenum depth, and inlet configuration. This section details our effort.

5.1 The effect of U-value of the diffuse ceiling panels

Two types of diffuse ceiling panels were compared regarding their impact on system performance under different operating conditions. One was wood-cement panel, and the other was Al panel. The Al panel had a thickness of 5 mm and thermal conductivity of 202.4W/m.K, corresponding to a U-value of 40480 W/m^2. K. The U-value of wood-cement panel was only 2.43 W/m^2.K. In order to limit the number of variables, it was assumed that both panels have the same porosity and the same pressure resistance. In addition, to avoid the influence of different emissivity on the radiative heat exchange, it was assumed that the Al panel is painted black and has the same emissivity as the wood-cement panel.

Table 3

Table 3 presents the CFD results with the two diffuse ceiling panels. From the standpoint of energy performance, the diffuse ceiling panel with a higher U-value was benefitical to the cooling capacity of radiant ceiling. A 22% enhancement on the cooling capacity was achieved by Al panels than that of wood-cement panels. Al panels increased both the convective heat transfer between radiant ceiling and plenum air, and the radiative heat transfer between radiant ceiling and diffuse ceiling panels. However, the opposite effect was found in the heating mode, where the heating capacity of radiant ceiling was reduced by 13%. Both convective and radiative heat exchange were reduced by Al panels. The reductions were due to Al panels decreased air-to-surface temperature difference and surface-to-surface temperature difference in the winter case. In the moderate season, the radiant ceiling was not activated. The diffuse ceiling had an indirect influence on the heat conducted from the floor above. The Al panels restricted the amount of heat transfer from the upper floor and maintained a slightly lower indoor temperature than did the wood-cement panels.

According to previous studies (Yu et al. 2015; Zhang et al. 2015a), the diffuse ceiling ventilation promotes the heating capacity of radiant ceiling but decreases its cooling capacity in comparison with the stand-alone radiant system. The heat transfer coefficient of cooled ceiling was measured to be 2.5 W/m^2.K with the diffuse ceiling (wood-cement panels), while the value without the diffuse ceiling was about 7.7 W/m^2.K. The reduction on the cooling capacity limited the amount of heat load can be removed by the system, and limited the application of the integrated system in the cooling season.

The results of the parametrical study indicated that diffuse ceiling panels with a higher U-value can minimize the negative impact and enable the radiant ceiling to cool down the room efficiently. It is recommended to utilize diffuse ceiling panels with a high U-value, if cooling is the primary task of the system.

The U-value of diffuse ceiling panels did not show a notable impact on the airflow pattern. Therefore, detailed comparisons of the velocity and temperature distributions were not discussed here.

5.2 The effect of plenum height

The study was performed on plenums varying from 5 cm to 35 cm in height under the boundary conditions of the winter case. The winter case was chosen as an example because the cold outdoor air would cause deterioration of the uniform air distribution through the diffuse ceiling and would enhance the draught risk in the occupied zone, see Figure 10 (a). Thus, this case is more critical than the others.

As depicted in Table 3, the reduction in the plenum height had a positive effect on the energy efficiency of the radiant ceiling. The convective heat transfer from the radiant ceiling to the plenum increased from 205 W to 461 W when the plenum height decreased from 35 cm to 5 cm. The low-height plenum forced cold supply air to contact the warm radiant surface directly with a high velocity, which enhanced both the convective coefficient and the air-to-surface temperature difference. As a result, the convective heat exchange increased dramatically. Although the radiant heat transfer from the radiant ceiling decreased because of the change in the diffuse ceiling surface temperature and view factors, the total heating capacity still increased from 516 W to 636W as the plenum height was reduced from 35 cm to 5 cm. Consequently, the air temperature in the room increased by approximately 3 ^{o}C.

Regarding air distribution, low-height plenum reduced the uniformity of supply flow through the diffuse ceiling. Figure 12 (a) illustrates the delivered airflow ratio through the diffuse ceiling. A uniform distribution would result in a delivered airflow ratio of 100% at all distances from the inlet. In all cases, high proportions of air were delivered at a short distance from the plenum inlet, and the air delivery gradually decreased as the distance from the plenum inlet increased. Furthermore, the reduction in plenum height exacerbated the situation. The distribution variation exceeded 120% with the 5 cm plenum, while the variation for the 35 cm plenum was less than 100%. The large distribution variation can be attributed to the low-pressure drop through the diffuse ceiling panels and also to the extremely low supply-air temperature.

Another important design consideration is the need to minimize the variation in supply air temperature. Figure 12 (b) shows temperature distribution just above the diffuse ceiling, which could present the supply air temperature. Because of the heat exchange with the radiant ceiling, the thermal decay on the supply air was significant in all cases. However, the low height plenum limited the mixing of air in the plenum and aggravated the temperature variation. When the plenum as low as 5 cm, the cold outdoor air formed downward supply flow and was delivered to the room directly, no mixing could be expected in this case.

Figure 12

Plenum height influences the air distribution through the diffuse ceiling, and further affects the flow behavior in the occupied zone. The velocity distributions at a height of 0.1 m were analyzed and compared under different plenum heights, as illustrated in Figure 13. When the plenum height decreased, reverse flow penetrated from the front of the room to the entire room, and the air velocity increased significantly. The air velocity exceeded 0.29 m/s in the case with 5 cm plenum height, which would result in a draught problem. The asymmetric distribution of velocity along the y-axis can be attributed to two factors. First, the exhaust was at the left corner of the façade (x = 0, y = 3.1, z = 0.25), which to some extent impacted the local air

velocity. Second, because of the random and asymmetric nature of the turbulent flow, the airflow would not have produced a perfectly symmetric pattern (Jin et al. 2006).

Figure 13

Although the temperature variation in the plenum reached 30 ºC, the air temperature in the occupied zone was very uniform. An effective mixing between supply air flow and convective flow from heat sources was observed. In order to keep this article brief, the plot of temperature distribution in the occupied zone will not be presented here.

5.3 The effect of plenum depth

The effect of plenum depth on the air distribution was investigated by doubling the depth, and its effect on the radiant ceiling energy performance was also discussed here. Because the room geometry was doubled, the heat loads were doubled accordingly and were located symmetrically along the x-axis. In addition, the air flow rate was doubled to maintain the ACH of 2 h^{-1}. Plenum height was kept at 35 cm, as in the experimental measurements. Only the winter case was studied, as for the reason discussed in Section 5.2.

The doubled plenum depth did not result in an exact doubling of the heat released from the radiant ceiling, as shown in Table 3. The total heat flow of the radiant ceiling was 965 W when the depth of the room was 9.6 m, which was only 87% greater than that of 4.8 m. As expected, both air velocity and temperature differences decreased as the air traveling further in the plenum. Consequently, both convective and radiative heat fluxes were weakened by the increase in plenum depth.

Figures 14 showed that doubling the plenum depth causes deterioration in the uniformity of the air distribution through the diffuse ceiling. The variation reached 140% when the room length was 9.6 m, while the variation in the 4.8 m case was less than 100%. Furthermore, it can be observed that there were two "jumps" in the curve at distances of approximately 2.2 m and 6.7 m from the plenum inlet. These jumps were because that the rising thermal plume reached the diffuse ceiling and acted as thermal blockages for the ventilation air flow. Therefore, low air delivery was found at these two locations. The temperature variation increased 3 ºC by doubling the plenum depth. The degree of temperature variation was determined by the amount of heat transfer from the thermal mass and also by the residence time of the supply air within the plenum. The greater the travel distance of the supply air, the larger the temperature variation will be.

Figure 14

The uneven supply flow further affected the flow behavior in the occupied zone. In this case, the high draught region penetrated to half of the room deep and the air velocity reached to 0.32 m/s, as seen in Figure 15. The occupants situated near the façade experienced significantly greater draught than the ones located near the back wall. The temperature variation along the length of the room was negligible (less than 1 ºC). From the standpoint of both energy efficiency and thermal comfort, it can be concluded that the integrated system is suitable to use in a small space, for instance, a single office room.

Figure 15

5.4 Effect of plenum inlet configuration

Two inlet configurations were studied, as illustrated in Figure 16. The original inlet setup served as a reference, where the glazing opening was simplified as a slot opening located just above the diffuse ceiling.

The other configuration was a square opening located at one corner of the plenum, which simulated a duct opening. The reason for constructing a square opening instead of a round one was to simplify the mesh. Both inlets had the same effective opening area, and the plenum height was 35 cm in both cases.

Figure 16

From the standpoint of energy performance, the squared opening slightly enhanced the energy efficiency of the radiant ceiling by increasing the convective heat exchange, as shown in Table 3. This can attribute to the location of the plenum inlet. The slot opening was located just above the diffuse ceiling, resulting in the distribution of cool supply air along the ceiling panels. The square opening was located closer to the radiant surface, where the cool supply air had more contact with the warm radiant surface, which led to greater heat exchange. The increase in the heating capacity resulted in a slight increase in the air temperature in both the plenum and the occupied space.

A plot of velocity distribution just above the diffuse ceiling supply is shown in Figure 17. Different flow patterns were generated by using different inlet configurations, as illustrated by the streamline. For the square opening, high velocity was observed in the corner of the plenum because of its centralized configuration. The slot opening enabled the injected air to be evenly distributed along the y- direction. The air velocity gradually decreased as the air traveled along the plenum, and the minimum velocity was at the far end of the plenum. The temperature variation of the delivered air was more significant with the square inlet, where the maximum delivered air temperature was 27.7 ^{o}C and the minimum temperature was 8.1 ^{o}C. The values for the reference inlet were 27.1 ^{o}C and 11.8 ^{o}C, respectively. To keep this article brief, a plot of the temperature distribution is not shown here.

Figure 17

Figures 18 present the velocity distributions at 0.1 m height in the room with the square opening. A large amount of air delivered in the corner through diffuse ceiling caused the penetration of airflow into the occupied zone at the corner of the room. However, high air velocity occurred only near the wall and did not increase the local draught risk. The maximum air velocity in the occupied zone was similar to that in the reference case, which was approximately 0.18 m/s. The lowest air temperature occurred in the corner, although the air temperature difference in the occupied zone was still less than 1 ^{o}C.

Figure 18

6. Conclusions

The objective of this study was to develop a numerical model for a combined system with diffuse ceiling supply and radiant ceiling. The air diffusion through the diffuse ceiling was simulated by a porous media model. The radiative heat exchange was calculated by a separate radiation model, and then was applied as boundary conditions for the porous media model. The numerical model was validated by measured results from a full-scale test facility under different operating conditions. The CFD results agreed well with the measured one on both temperature and velocity. This numerical model has been proved that it is able to use for predicting the airflow pattern and thermal performance in a room with the integrated system.

The validated numerical model was further applied in a series of parametric studies, to analyze the effects of selected design parameters. Several conclusions can be drawn:

1. The previous study indicated that the presence of diffuse ceiling increased the heating capacity of the radiant ceiling but decreased its cooling capacity. The cooling capacity of the integrated system was only one-third of the stand-alone radiant system, which limited the application of the integrated system in the cooling season. By comparing two diffuse ceiling panels, it was found that the panel with a higher U-value could reduce the impact on the energy performance of radiant ceiling, and made it possible to cool down the room efficiently.
2. The low height plenum enabled forced convection between supply air and radiant ceiling, and enhanced the energy efficiency of the system. However, the reduction in plenum height deteriorated the uniformity of air distribution through the diffuse ceiling and resulted in a higher draught in the occupied zone.
3. Increase plenum depth had negative impacts on the energy performance of radiant ceiling and the thermal comfort in the occupied zone. The results indicated that the integrated system is suitable to apply in small offices rather than large, open spaces.
4. The plenum inlet configuration had impacts on the air distribution in both the plenum and the occupied zone. To enhance the energy efficiency of the radiant ceiling, plenum inlet should be placed close to the radiant surface.

Compared with conventional radiant ceiling and separated ventilation system, the two subsystems interact and complement with each other in the integrated system. The system showed a promising opportunity as a heating system and the potential to use the natural cooling resource without compromise thermal comfort. However, a reduction in the cooling capacity could not be neglected. A dynamic state investigation would be interesting in the further study, which focuses on the night cooling potential and the thermal storage capacity of the ceiling slab and diffuse ceiling panel.

Nomenclature

C_2 inertial resistance factor [1/m]

E_f total fluid energy [m^2/s^2]

F_{kj} view factor between surfaces k and j

k_{eff} effective thermal conductivity of the medium [W/m.K]

k_f fluid thermal conductivity [W/m.K]

k_s solid medium thermal conductivity [W/m.K]

P pressure [Pa]

q_{rad} radiative heat flux [W/m^2]

S_M momentum source term [N/m^3]

S_E energy source term [W/m^3]

V superficial velocity [m/s]

α permeability [m^2]

ε_k emissivity

μ dynamic viscosity [kg/m.s]

γ porosity of the medium

ρ air density [kg/m^3]

ρ_k reflection coefficient

τ shear stress [Pa]

σ Stefan-Boltzmann constant, 5.67*10^{-8} [W/m^2.K^4]

References

ANSYS Inc. (2015). Ansys Fluent release 16.0. Available at: http://www.ansys.com/.

ANSYS Inc. (2009). *ANSYS FLUENT User's Guide*.

Arcuri N, Bruno R, Bevilacqua P (2015). Influence of the optical and geometrical properties of indoor environments for the thermal performances of chilled ceilings. *Energy and Buildings*, 88: 229–237.

ASHRAE (2009). ASHRAE Fundamentals Handbook (SI). Atlanta, Ga. : American Society of Heating Refrigerating and Air-Conditionin Engineers.

Bauman F (2013). Underfloor Air Distribution (UFAD) Design Guide. Atlanta, GA: American Society of Heating, Refrigerating and Air-Conditioning Engineers.

Brohus H (1998). Influence of a Cooled Ceiling on Indoor Air Quality in a Displacement Ventilated Room Examined by Means of Computational Fluid Dynamics. In: Proceedinga of the 6th International conference on air distribution in rooms, Stockholm, Sweden, pp. 53–60.

Causone F, Baldin F,Olesen B, Corgnati S (2010). Floor heating and cooling combined with displacement ventilation: Possibilities and limitations. *Energy and Buildings*, 42(12): 2338–2352. doi:10.1016/j.enbuild.2010.08.001.

CEN (1998). DS/CEN/CR 1752: Ventilation for buildings - Design criteria for the indoor environment.

Chen Q (1995). Comparison of Different K-E Models for Indoor Air Flow Computations. *Numerical Heat Transfer Part B Fundamentals An International Journal of Computation and Methodology*, 28(3): 353–369. doi: 10.1080/10407799508928838.

Chen Q, Srebric J (2002). A procedure for verification , validation , and reporting of indoor environment CFD analyses. *HVAC&R Research*, 8(2): 201–216. doi: 10.1080/10789669.2002.10391437.

Chodor A , Taradajko P (2013). Experimental and Numerical Analysis of Diffuse Ceiling Ventilation. Master Dissertation, Department of Civil Engineering, Aalborg University, Denmark.

Fan J, Hviid C, Yang H (2013). Performance analysis of a new design of office diffuse ceiling ventilation system. *Energy and Buildings*, 59:73–81. doi:10.1016/j.enbuild.2013.01.001.

Hviid C, Svendsen S (2013). Experimental study of perforated suspended ceilings as diffuse ventilation air inlets. *Energy and Buildings*, 56: 160–168. doi:10.1016/j.enbuild.2012.09.010

Jacobs P, Knoll B (2009). Diffuse ceiling ventilation for fresh classrooms. In: Proceedings of the 4 th Intern. Symposium on Building and Ductwork Air tightness, Berlin, Germany, pp. 1–7.

Jacobs P, Oeffelen E, Knoll B (2008). Diffuse ceiling ventilation, a new concept for healthy and productive classrooms. In: Proceedings of the 11th International Conference on Indoor Air Quality and Climate,

Copenhagen, Denmark, pp. 17–22.

Jakubowska E (2007). Air distribution in rooms with the diffuse ceiling inlet. Master Dissertation, Department of Civil Engineerging, Aalborg University, Denmark.

Jin H, Bauman F, Webster T (2006). Testing and modeling of underfloor air supply plenums. *ASHRAE Transactions*, 112(2): 581–591.

Krajčík M, Tomasi R, Simone A (2013). Experimental study including subjective evaluations of mixing and displacement ventilation combined with radiant floor heating/cooling system. *HVAC&R Research*, 19(8):1063–1072. doi: 10.1080/10789669.2013.806173.

Myhren J, Holmberg S (2008). Flow patterns and thermal comfort in a room with panel, floor and wall heating. *Energy and Buildings*, 40(4): 524–536. doi:10.1016/j.enbuild.2007.04.011.

Nielsen P, Jakubowska E (2009). The Performance of Diffuse Ceiling Inlet and other Room Air Distribution Systems. In: Proceedings of COLD CLIMATE HVAC, Sisimiut, Greenland.

Niu J, Kooi J (1994). Indoor climate in rooms with cooled ceiling systems. *Building and Environment*, 29(3): 283–290. doi:10.1016/0360-1323(94)90024-8.

Novoselac A, Srebric J (2002). A critical review on the performance and design of combined cooled ceiling and displacement ventilation systems. *Energy and Buildings*, 34(5): 497–509. doi:10.1016/S0378-7788(01)00134-7

Petersen S, Christensen N, Heinsen C, Hansen A (2014). Investigation of the displacement effect of a diffuse ceiling ventilation system. *Energy and Buildings*, 85, pp.265–274. doi:10.1016/j.enbuild.2014.09.041.

Rees S, Haves P (2013). An experimental study of air flow and temperature distribution in a room with displacement ventilation and a chilled ceiling. *Building and Environment*, 59:358–368. doi:10.1016/j.buildenv.2012.09.001

Riffat S, Zhao X, Doherty P (2004). Review of research into and application of chilled ceilings and displacement ventilation systems in Europe. *International Journal of Energy Research*, 28(3): 257–286. doi: 10.1002/er.964

Srebric J, Chen Q (2002). An example of verification , validation , and reporting of indoor environment CFD analyses (RP-1133). *ASHRAE Transactions*, 108(2):185–194.

Su L, Zhang X, Sun Y, Qian J (2015). Heat transfer and cooling characteristics of concrete ceiling radiant cooling panel. *Applied Thermal Engineering*, 84: 170–179. doi:10.1016/j.applthermaleng.2015.03.045.

Tye-Gingras M, Gosselin L (2012). Comfort and energy consumption of hydronic heating radiant ceilings and walls based on CFD analysis. *Building and Environment*, 54: 1–13. doi:10.1016/j.buildenv.2012.01.019.

Yang Y, Chen C (2008). Numerical simulation of turbulent fluid flow and heat transfer characteristics of heated blocks in the channel with an oscillating cylinder. *International Journal of Heat and Mass Transfer*, 51(7-8):.1603–1612. doi:10.1016/j.ijheatmasstransfer.2007.07.010.

Yu T, Heiselberg P, Lei B, Pomianowski M, Zhang C, Jensen R (2015). Experimental investigation of cooling performance of a novel HVAC system combining natural ventilation with diffuse ceiling inlet and TABS. *Energy and Buildings*, 105: 165–177. doi:10.1016/j.enbuild.2015.07.039.

Zhang C, Heiselberg P, Pomianowski M, Yu T, Jensen R (2015a). Experimental study of diffuse ceiling ventilation coupled with a thermally activated building construction in an office room. *Energy and Buildings*, 105: 60–70. doi:10.1016/j.enbuild.2015.07.048.

Zhang C, Heiselberg P, Pomianowski M, Yu T, Jensen R (2015b). Integrated solution in an office room with diffuse ceiling ventilation and thermally activated building constructions. *Energy Procedia*, 78:2808–2813. doi:10.1016/j.egypro.2015.11.635.

Zhang C, Kristensen M, Jensen J, Heiselberg P, Jensen R, Pomianowski M (2016). Parametrical analysis on

the diffuse ceiling ventilation by experimental and numerical studies. *Energy and Buildings*, 111: 87–97. doi:10.1016/j.enbuild.2015.11.041.

Figure and Table

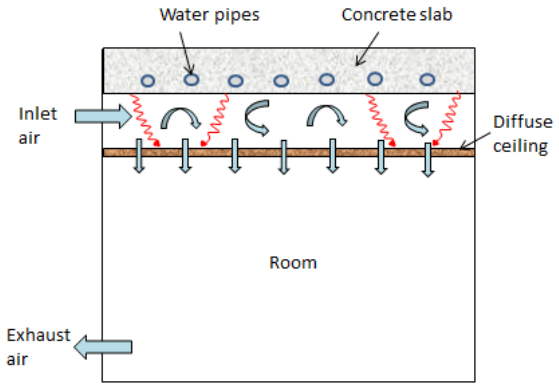

Fig.1 Schematic diagram of the integrated system

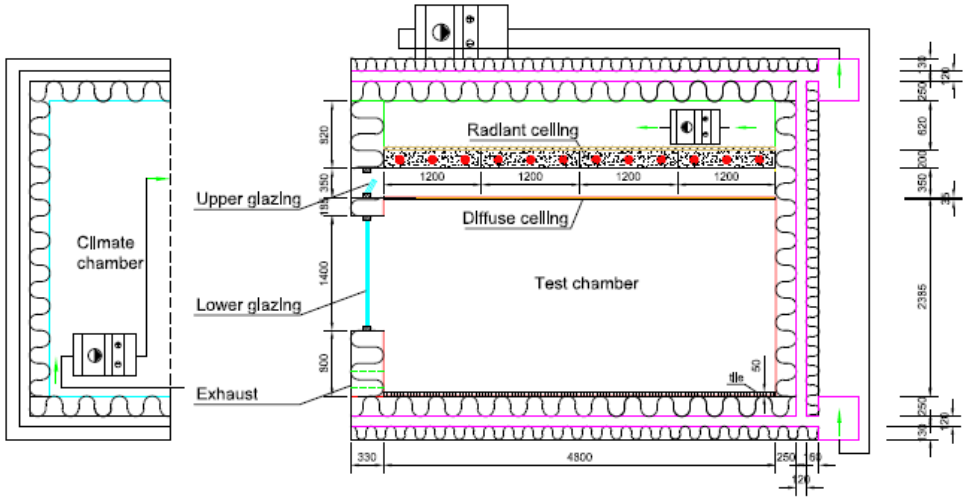

Fig.2. Vertical section view of environmental chamber

Fig.3. The test chamber with an office layout

Fig.4. Diffuse ceiling panels and radiant ceiling

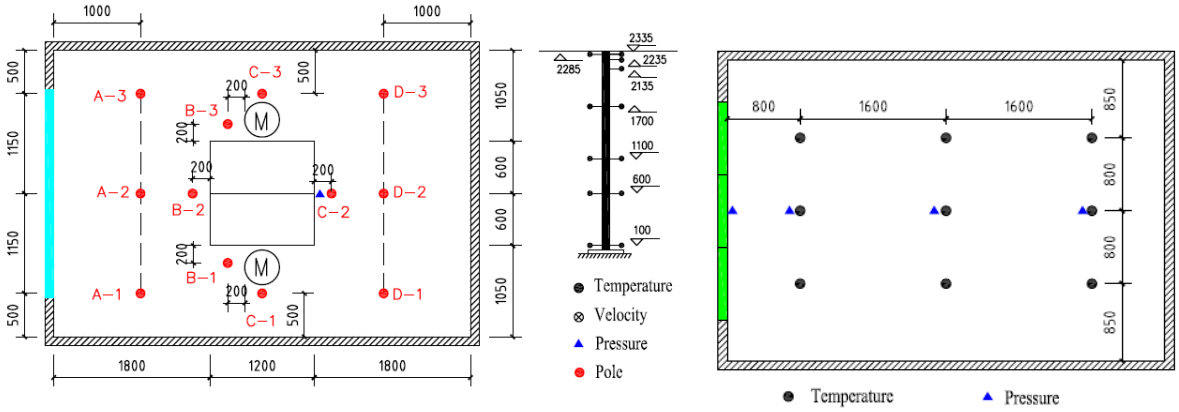

(a) (b)

Fig. 5 Measuring locations in plan view (a) Office (b) Plenum

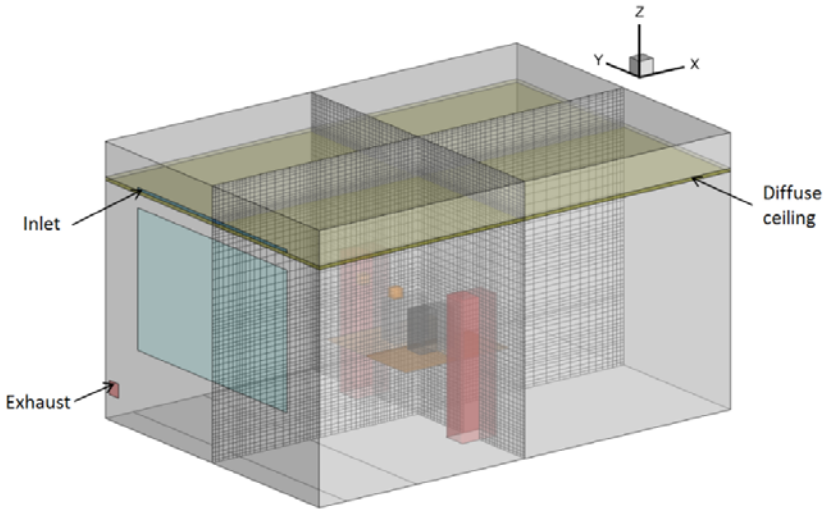

Fig.6. Geometrical model and mesh distribution of the integrated system in an office room

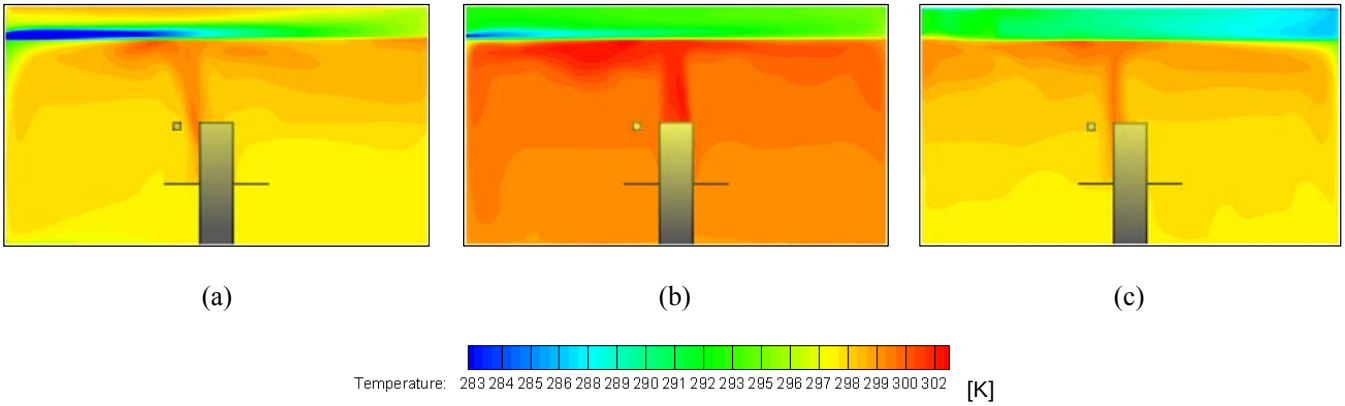

Fig.7. Temperature distribution across the central plane (a) Winter, (b) Moderate season, and (c) Summer

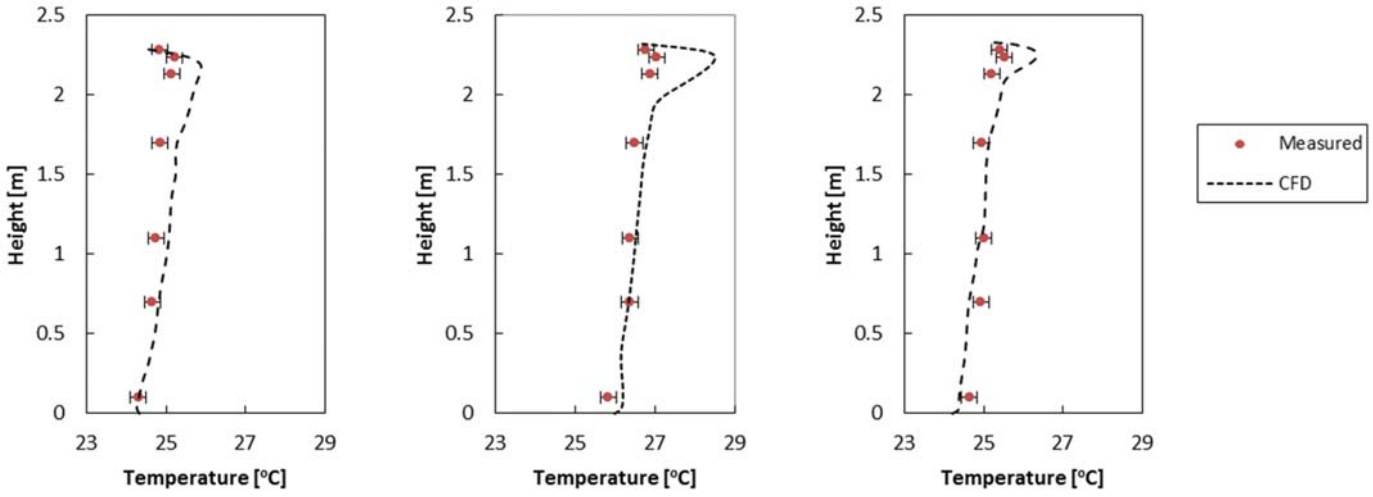

(a) (b) (c)

Fig.8. Vertical temperature profile at A2: (a) Winter, (b) Moderate season, and (c) Summer

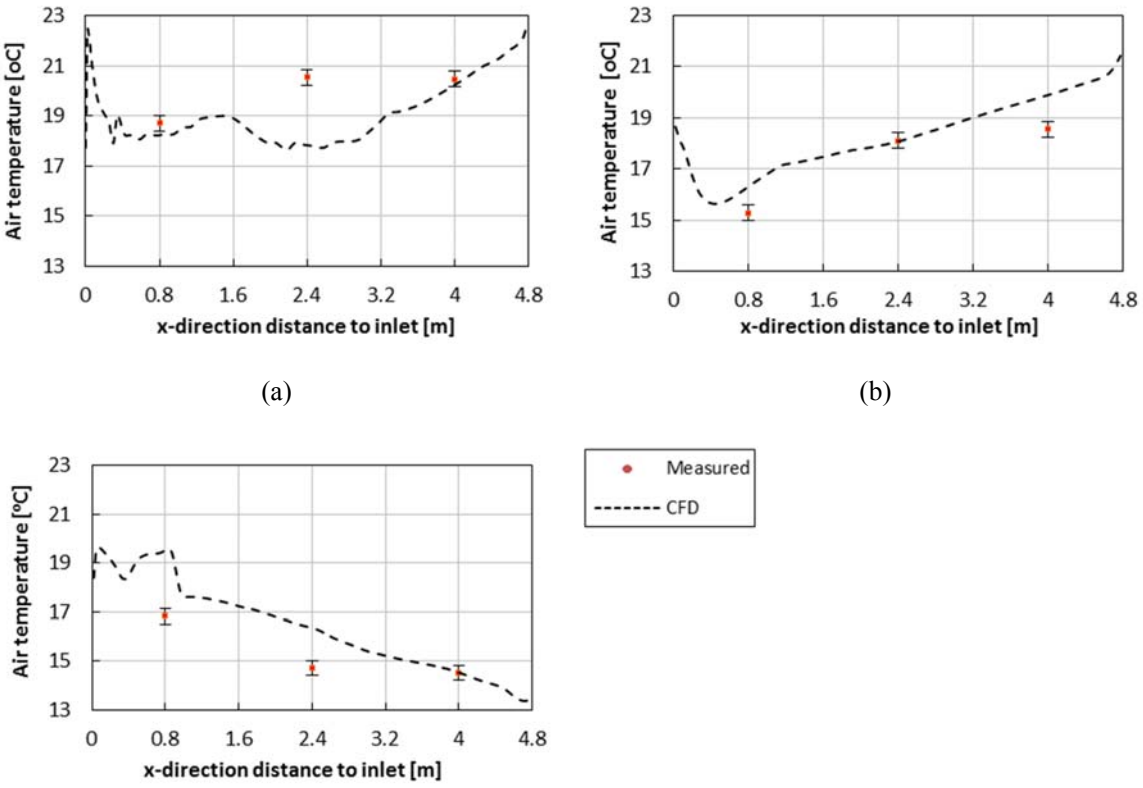

(a) (b)

(c)

Fig.9. Air temperature distribution at the mid-height of the plenum: (a) Winter, (b) Moderate season, and (c) Summer

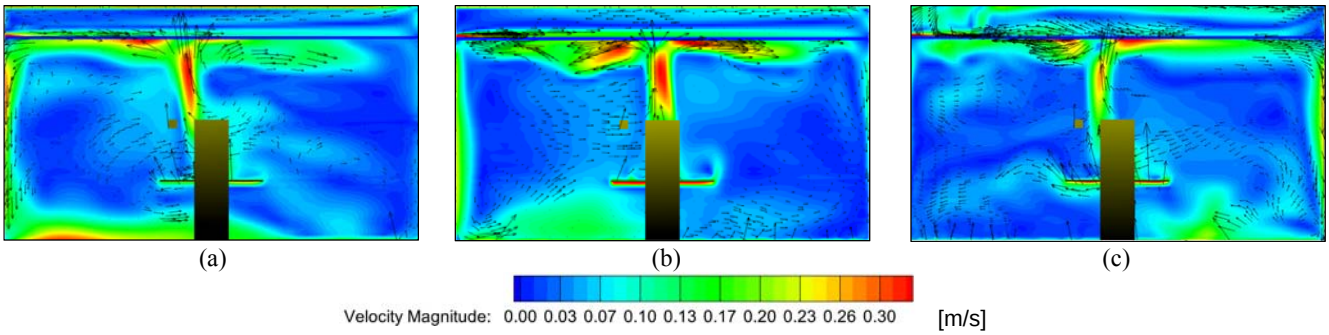

(a) (b) (c)

Fig.10. Velocity vector across the central plane: (a) Winter, (b) Moderate season, and (c) Summer

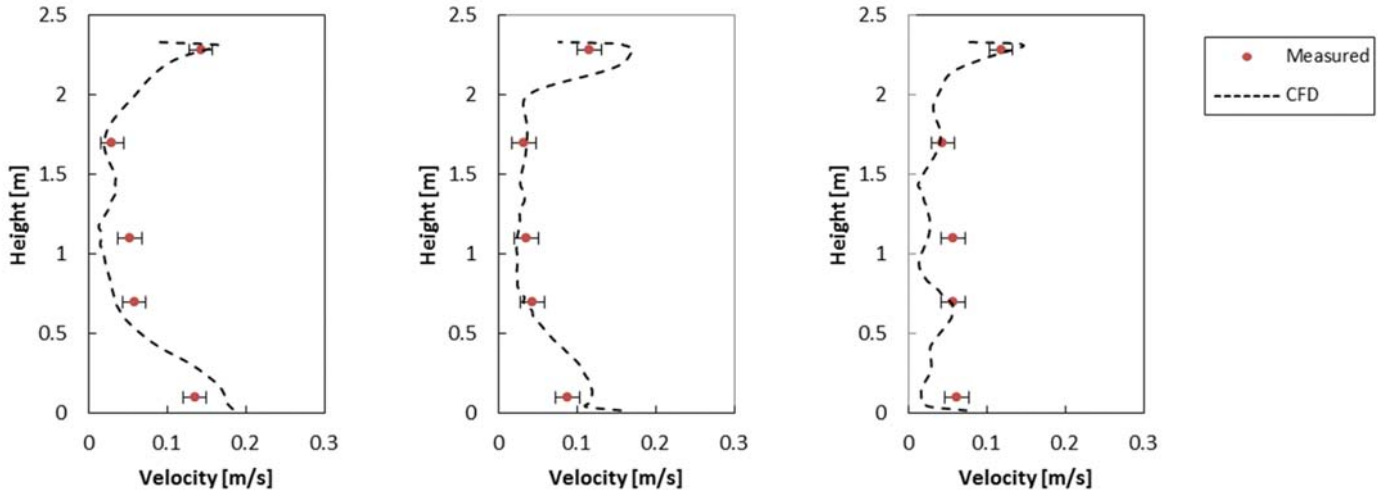

(a) (b) (c)

Fig.11. Vertical velocity profile at A2: (a) Winter, (b) Moderate season, and (c) Summer

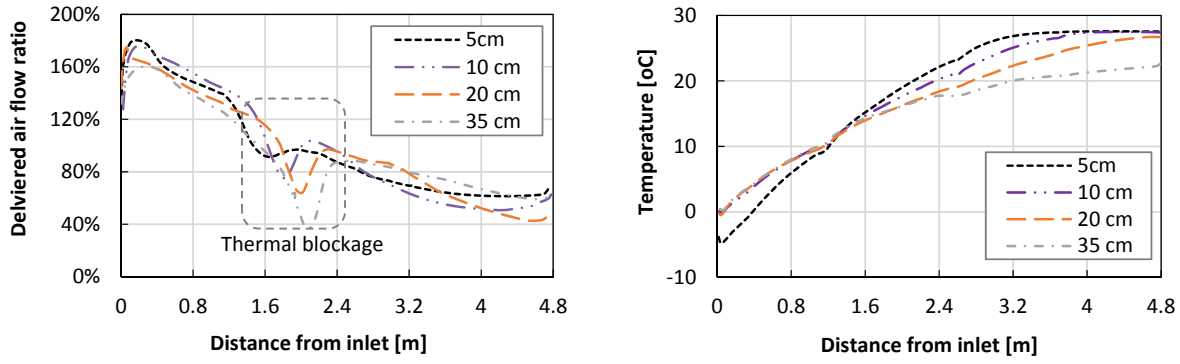

(a) (b)

Fig. 12. Air distribution through the diffuse ceiling with different plenum heights (a) Delivered air flow ratio (b) Temperature distribution

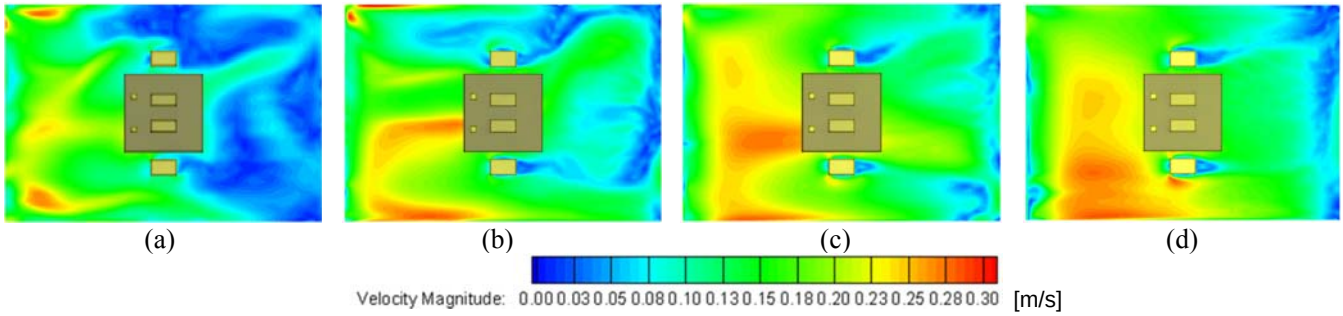

Fig. 13. Velocity distribution at a height of 0.1 m with different plenum heights: (a) 35 cm, (b) 20 cm, (c) 10 cm, and (d) 5 cm

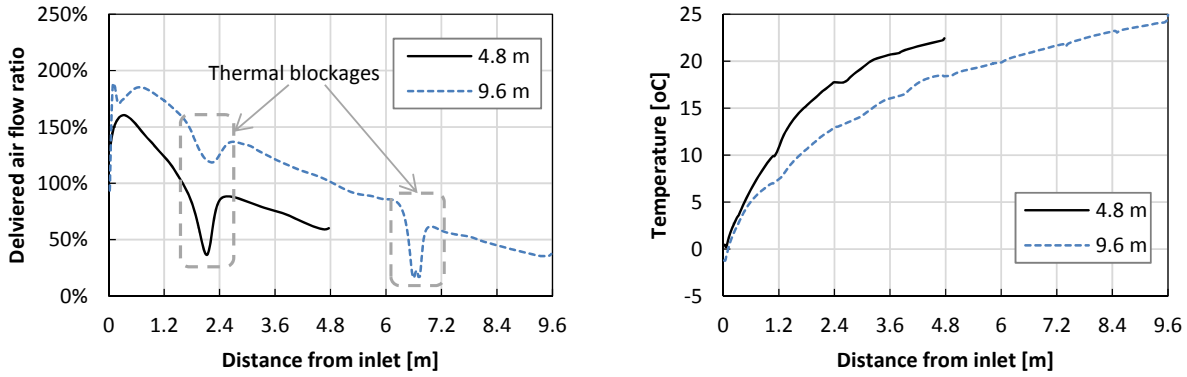

(a) (b)

Fig. 14. Air distribution through the diffuse ceiling with different plenum depths (a) Delivered air flow ratio (b) Temperature distribution

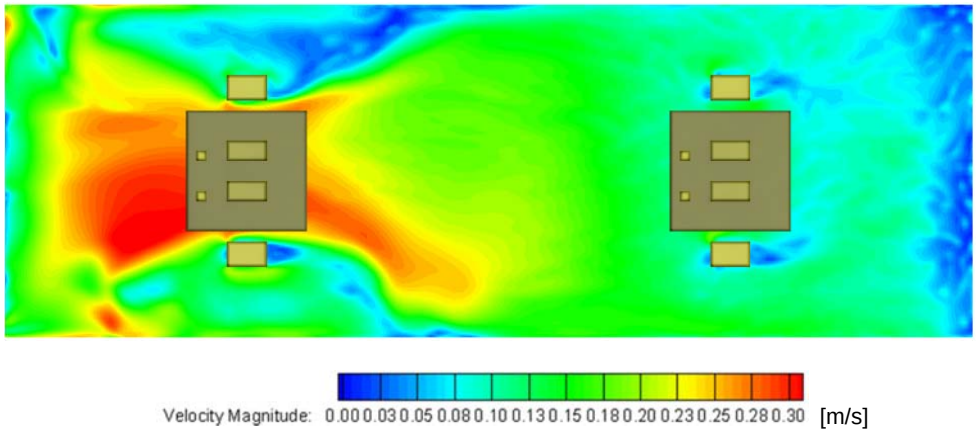

Fig.15. Velocity distribution at a height of 0.1 m in the room with doubled depth

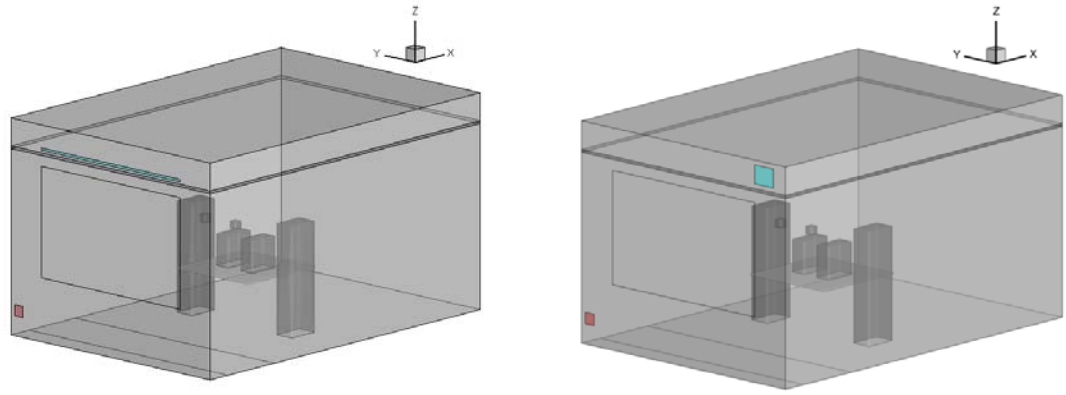

(a) (b)

Fig. 16. Plenum inlet configurations: (a) slot opening and (b) square opening

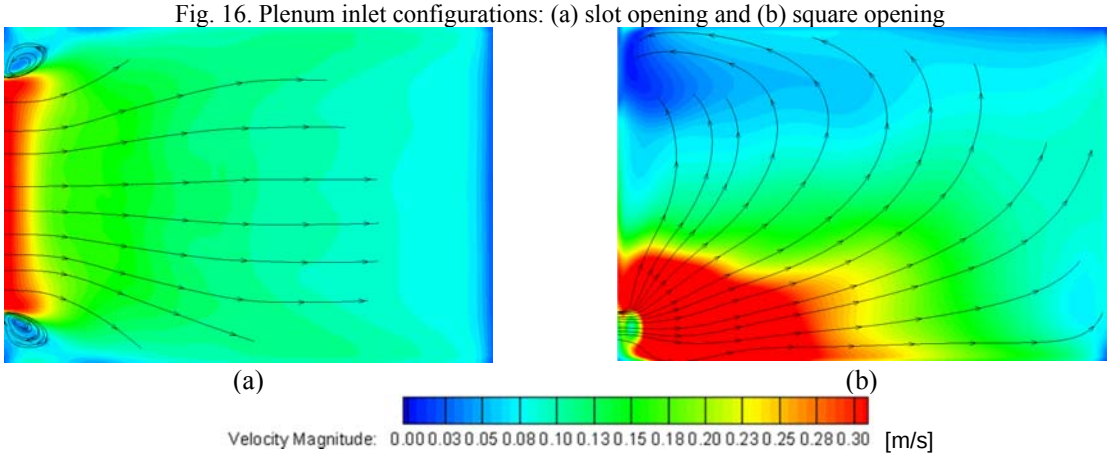

(a) (b)

Fig. 17. Velocity distribution above the diffuse ceiling with different plenum inlet configurations: (a) slot opening and (b) squared opening

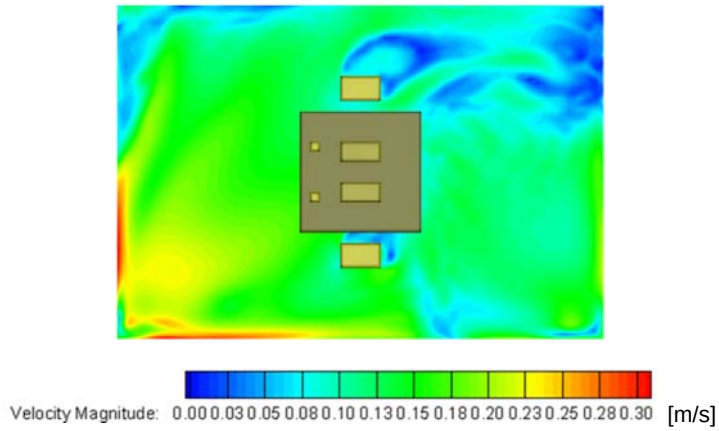

Fig. 18. Velocity distribution at a height of 0.1 m with the square opening

Table 1. Test conditions for the three cases

Case	ACH	Supply air temp.	Radiant ceiling surface temp.	Interior heat load
	h^{-1}	°C	°C	W
Winter	2	-6.87	27.34	450.5
Moderate season	2	9.46	-	450.5
Summer	2	24.10	10.79	450.5

Table 2. Grid independence study

Variable	Mesh 1	Mesh 2	Mesh 3
Number of cells	353,312	760,235	1,027,309
Exhaust air temperature [°C]	25.95	26.25	26.28
Air velocity at A2 [m/s]	0.065	0.068	0.068
Mass unbalance [kg/s]	0.00	0.00	0.00
Heat flux unbalance [W]	0.56	0.89	0.40
Heat flux unbalance [%]	-0.12%	-0.20%	-0.09%

Table 3. CFD results with different design parameters

Design Parameter		Operating condition		CFD calculated results				
	Description	Supply air temp.	Radiant ceiling surface temp.	Plenum air temp.	Room air temp.	Radiant ceiling heating/cooling capacity	Radiant ceiling radiative heat flow	Radiant ceiling convective heat flow
		°C	°C	°C	°C	W	W	W
Diffuse ceiling panel	Wood-cement	-6.87	27.34	18.70	25.11	516.61	311.52	205.09
	Al			20.24	23.62	449.68	258.69	190.99
	Wood-cement	9.46	-	19.55	26.72	-	-	-
	Al			22.20	25.94	-	-	-
	Wood-cement	24.10	10.79	16.56	24.46	-461.11	-172.29	-288.82
	Al			17.48	22.17	-556.74	-235.98	-320.76
Plenum height	35 cm	-6.87	27.34	18.70	25.11	516.61	311.52	205.09
	20 cm			18.82	26.04	540.10	272.66	267.44
	10 cm			19.00	27.94	603.86	203.88	399.98
	5 cm			20.36	28.76	636.44	175.08	461.37
Plenum depth	4.8 m	-6.87	27.34	18.70	25.11	516.61	311.52	205.09
	9.6 m			18.58	25.05	965.03	576.07	388.96
Plenum inlet	Original	-6.87	27.34	18.70	25.11	516.61	311.52	205.09
	Corner			19.33	25.32	540.67	294.28	246.39